SIMULATION OF RAMAN FREE-ELECTRON LASER AMPLIFIER WITH PLANAR WIGGLER AND ION CHANNEL GUIDING

B. Maraghechi # and M. H. Rouhani
Department of Physics, Amirkabir University of Technology, P. O. Box 15875-4413, Tehran, Iran.

Abstract

A local and nonlinear simulation of the Raman free-electron laser amplifier with a planar wiggler, and ion-channel guiding is presented. Using Maxwell's equations and full Lorentz force equation of motion for the electron beam, a set of coupled nonlinear differential equations is derived in slowly varying amplitude and wave number approximation and is solved numerically. The electron beam is assumed cold, propagates with a relativistic velocity, ions are assumed immobile and slippage is ignored. Ion-channel density is varied and the results for group I and II orbits are compared with the case when the ion channel is absent. It is found that by using an ion channel, growth rate can be increased, saturation length can be decreased, and the saturated amplitude of the radiation can be increased.

INTRODUCTION

For low energy but high current electron beams, a focusing mechanism is required in order to confine the beam against the self-fields. In ion focusing technique, the beam space charge quickly ejects the electrons of a pre-ionized plasma leaving an ion core. The presence of ions neutralizes the beam space charge, and thus overcomes the beam divergence caused by its self fields. Since the pulse duration of beams in FEL is typically rather short, it is assumed that ions are immobile and hosing instability is absent [1].

This technique was first proposed by Takayama and Hiramatsu for use in FELs [2]. It was first demonstrated experimentally by Ozaki et al. [3] and investigated via numerical simulation by Yu et al. [4] and by Jha and Wurtele [5]. Analysis in Ref. [4] indicates that the combination of ion focusing and beam conditioning permits high gain in the soft x-ray regime. In Ref. [5], an averaged three-dimensional code has been developed for the FEL simulation that allows for the effects of an ion channel but in that code the effect of ion channel on the variation of energy was ignored i.e., the dot product of the transverse velocity with the electric field of the ion-channel was not considered in Eq. (4) of Ref. [5]. Moreover, the effect of radiation on the transverse motion was not considered in Eq. (2) of Ref. [5]. Therefore, a very limited effect of the ion channel was considered therein.

Recently, the nonlinear dynamics of a single-pass FEL in presence of an ion channel for helical wiggler has been studied [6]. In this article, injection of electrons into the wiggler has not been considered.

The purpose of the present study is to present a non-averaged and nonlinear simulation of a FEL in the planar wiggler with ion-channel guiding in the Raman regime, using the simulation technique of Ref. [7]. It is important to emphasize that following Freund [7], no average is performed over the Lorentz force equation, therefore, the Kroll-Morton-Rosenbluth (KMR) scheme is not used [8]. In the KMR method [4, 5, 8-10], electron trajectories are averaged over the wiggler period. Hence, only two equations are integrated per electron; specifically, for the energy and ponderomotive phase.

FIELD STRUCTURE AND ELECTRON DYNAMICS

The idealized tapered and planar wiggler magnetic field may be described by

$$\mathbf{B}_w(z) = B_w(z)\sin(k_w z)\hat{\mathbf{e}}_y , \tag{1}$$

$$B_w(z) = \begin{cases} B_w \sin^2\left[k_w z/(4N_w)\right] & 0 \le z \le N_w\lambda_w \\ B_w & N_w\lambda_w \le z \end{cases}$$

where $B_w(z)$ denotes the wiggler amplitude and $k_w = 2\pi/\lambda_w$ is the wiggler wave number. In the presence of an ion channel, the following transverse electrostatic field acts on an electron [11]

$$\mathbf{E}_i(x,y) = 2\pi n_i e\left(x\hat{\mathbf{e}}_x + y\hat{\mathbf{e}}_y\right) \tag{2}$$

where n_i is the number density of positive ions with charge e. The vector and scalar potential of radiation and the space charge wave are written as

$$\delta\mathbf{A}(z,t) = \delta A(z)\cos\alpha_+\hat{\mathbf{e}}_x , \tag{3}$$

$$\delta\phi(z,t) = \delta\phi(z)\cos\alpha , \tag{4}$$

$$\alpha_+ = \int_0^z k_+(z')dz' - \omega t , \tag{5}$$

$$\alpha = \int_0^z k(z')dz' - \omega t . \tag{6}$$

The amplitudes and wave numbers of the radiation and space-charge fields are assumed to vary slowly with z.

behrouz@aut.ac.ir

Equations governing dynamics of electrons may be derived by using relativistic equation of motion in the above mentioned fields. Using the dimensionless variables $\mathbf{u} = \mathbf{p}/mc = \gamma\boldsymbol{\beta}$, $\bar{x} = k_w x$, $\bar{y} = k_w y$, $\bar{k} = k/k_w$, $\bar{k}_+ = k_+/k_w$, $\bar{t} = tk_w c$, and $\bar{\omega} = \omega/k_w c$, these equations are

$$\frac{du_x}{d\bar{z}} = \bar{\Omega}_w(\bar{z})\sin(\bar{z}) - \bar{\omega}_i^2 \frac{\gamma \bar{x}}{u_z} + \delta a\left\{\frac{\gamma\bar{\omega}}{u_z} - \bar{k}_+\right\}\sin\alpha_+ + \frac{d\delta a}{d\bar{z}}\cos\alpha_+, \quad (7)$$

$$\frac{du_y}{d\bar{z}} = -\bar{\omega}_i^2 \frac{\gamma \bar{y}}{u_z}, \quad (8)$$

$$\frac{du_z}{d\bar{z}} = \bar{\Omega}_w(\bar{z})\frac{u_x}{u_z}\sin(\bar{z}) + \frac{\gamma}{u_z}\left(\frac{d\delta\varphi}{d\bar{z}}\cos\alpha - \bar{k}\delta\varphi\sin\alpha\right) - \frac{u_x}{u_z}\left(\frac{d\delta a}{d\bar{z}}\cos\alpha_+ - \bar{k}_+\delta a\sin\alpha_+\right), \quad (9)$$

where $\bar{\Omega}_w = eB_w/mk_w c^2$ is the undulator parameter, $\delta a = e\delta A/mc^2$, $\delta\varphi = e\delta\phi/mc^2$, and $\bar{\omega}_i^2 = 2\pi n_i e^2/mc^2 k_w^2$. Here α_+ and α evolve according to the following differential equations

$$d\alpha_+/d\bar{z} = \bar{k}_+ - \bar{\omega}\gamma/u_z, \quad (10)$$

$$d\alpha/d\bar{z} = \bar{k} - \bar{\omega}\gamma/u_z. \quad (11)$$

Note that the integration parameter is changed from $\bar{t}$ to $\bar{z}$, according to the relation $d/d\bar{t} = \beta_z d/d\bar{z}$. The differential equations governing the transverse electron motion are

$$d\bar{x}/d\bar{z} = u_x/u_z \quad (12)$$

$$d\bar{y}/d\bar{z} = u_y/u_z \quad (13)$$

It is worth to note that the variation of energy in this system is given by

$$mcd\gamma/dt = -e\boldsymbol{\beta}\cdot(\mathbf{E}_i + \delta\mathbf{E}_\perp + \delta E_z\hat{\mathbf{e}}_z).$$

In Ref. 5, the first term inside the parentheses in the above equation was left out. Also, for calculating the transverse velocity the effect of radiation was ignored and only the effect of wiggler was included. As shown in Ref 7, in the negative mass regime, the transverse velocity of electrons become large and, therefore, the first term in the above equation play an important role.

RADIATION DYNAMICS

In the Coulomb gauge, Maxwell equations can be written as [12]

$$\left(\partial^2/\partial\bar{z}^2 - \partial^2/\partial\bar{t}^2\right)\delta a = -4\pi\delta J_x(\bar{z},\bar{t}), \quad (14)$$

and

$$\partial^2\delta\varphi/\partial\bar{z}\partial\bar{t} = 4\pi\delta J_z(\bar{z},\bar{t}), \quad (15)$$

where $\delta\mathbf{J}(\bar{z},\bar{t})$ is the nonlinear current density and $\delta J_x(\delta J_z)$ is its component perpendicular to (along) the z-direction. The current density can be written as an average over the entry time $\bar{t}_0$ (defined as the time at which an electron crosses the $\bar{z} = 0$ plane)

$$\delta\mathbf{J}(\bar{z},\bar{t}) = -\frac{\bar{\omega}_b^2\beta_{z0}}{4\pi}\int_{-\infty}^{+\infty} d\bar{t}_0 \frac{\sigma(\bar{t}_0)\boldsymbol{\beta}(\bar{t},\bar{t}_0)\delta[\bar{t} - \tau(\bar{z},\bar{t}_0)]}{|\beta_z(\bar{t},\bar{t}_0)|}, \quad (16)$$

where $\bar{\omega}_b^2 = 4\pi n_b e^2/mk_w^2 c^2$, $\boldsymbol{\beta}(\bar{t},\bar{t}_0)$ is the velocity at time $\bar{t}$ of an electron, which has crossed the entry plane at time $\bar{t}_0$, $\sigma(\bar{t}_0)$ is the distribution in entry times, and

$$\tau(\bar{z},\bar{t}_0) = \bar{t}_0 + \int_0^{\bar{z}} \beta_z^{-1}(\bar{z}',\bar{t}_0)d\bar{z}' \quad (17)$$

Here, $\tau(\bar{z},\bar{t}_0)$ is the time that the electron reaches $\bar{z}$ and $\beta_z(\bar{z},\bar{t}_0)$ denotes the velocity of an electron at axial position z which crossed the entry plane at time $\bar{t}_0$. It is to be noted that in the definition of $\delta J(\bar{z},\bar{t})$ the electron beam is assumed to be mono-energetic and is characterized by a vanishing pitch-angle spread.

A set of coupled nonlinear differential equations for the slowly varying amplitudes and wave numbers is obtained by a straightforward substitution of Eqs. (3) and (4) into the Maxwell equations (14) and (15). The nonlinear Eq. (14) can be reduced to three first-order differential equations for δa, $\bar{\Gamma}_+$, and $\bar{k}_+$, where $\bar{\Gamma}_+$ defines the growth rate (logarithmic derivative). These equations are

$$d\delta a/d\bar{z} = \bar{\Gamma}_+\delta a, \quad (18)$$

$$d\bar{\Gamma}_+/d\bar{z} = -\bar{\omega}^2 - \bar{\Gamma}_+^2 + \bar{k}_+^2 + 2\bar{\omega}_b^2\beta_{z0}\left\langle u_x\cos\alpha_+/|u_z|\right\rangle/\delta a, \quad (19)$$

$$d\bar{k}_+ / d\bar{z} = -2\bar{k}_+\bar{\Gamma}_+ - 2\bar{\omega}_b^2\beta_{z0}\langle u_x \sin\alpha_+ / |u_z|\rangle / \delta a\,, \quad (20)$$

$$d\delta\varphi / d\bar{z} = -2\bar{\omega}_b^2\beta_{z0}\langle \sin\alpha\rangle / \bar{\omega}\,, \quad (21)$$

$$\bar{k} = -2\bar{\omega}_b^2\beta_{z0}\langle \cos\alpha\rangle / (\bar{\omega}\delta\varphi)\,. \quad (22)$$

Here, the average operator is defined over the initial ponderomotive phase $\psi_0 = -\bar{\omega}\bar{t}_0$ as

$$\langle(\cdots)\rangle = \frac{1}{2\pi}\int_{-\pi}^{+\pi} d\psi_0\sigma(\psi_0)(\cdots), \quad (23)$$

where the ponderomotive phase is $\psi = (k_w + k)z - \omega t = \alpha_+ + k_w z$. This is an average over a beamlet of electrons which cross the entry plane within one wave period. In the derivation of the above equations the wave equations (14) and (15) have been averaged over the wave period and the source currents and charge densities substituted. Moreover, by using a symmetry argument that electrons that enter the interaction regime at time intervals equal to $2\pi N/\omega$, with N an integer, will have identical trajectories, the integral limits on t and t_0 are exchanged [12, 13].

NUMERICAL SOLUTION

Equations (7)-(13) together with Eqs. (18)-(21) form a set of $7N+4$ self-consistent first-order differential equations, where N stands for the number of electrons. The common parameters, which are used, correspond to a situation in which $\bar{\Omega}_w/\gamma = 0.04$, $\gamma = 7$, $\bar{\omega}_b/\sqrt{\gamma} = 0.08$, $\delta a(\bar{z}=0) = 10^{-7}$, and an entry taper of $N_w = 10$ wiggler periods.

For un-bunched electron beam the particles are uniformly distributed in phase for $0 \le \psi_0 \le 2\pi$. The initial conditions of wave fields are chosen to have resonance conditions according to the linear theory. Since the wiggler field increases adiabatically from zero at the entry plane, the growth rate of the vector potential is initially zero as well. Wave numbers of the vector and scalar potentials are chosen to satisfy the uncoupled dispersion equations. The linearly polarized electromagnetic wave satisfies the following dispersion relation [14]

$$\bar{\omega}^2 - \bar{k}_+^2 - \left[\bar{\omega}_b^2(\bar{\omega} - \bar{k}_+\beta_{z0})^2\right] / \left[\gamma_0(\bar{\omega} - \bar{k}_+\beta_{z0})^2 - \bar{\omega}_i^2\right] = 0 \quad (24)$$

in the presence of ion channel. The dispersion relation for the negative energy space-charge wave is

$$(\bar{\omega} - \beta_{z0}\bar{k}) = -\bar{\omega}_b / \gamma_0^{1/2}\gamma_{z0}\,. \quad (25)$$

The equilibrium trajectories are studied in Ref. 15 and two types of orbits are found for different ion-channel densities. For the group I orbits $\bar{\omega}_i^2 < \gamma_0\beta_{z0}^2$ and for the group II orbits $\bar{\omega}_i^2 > \gamma_0\beta_{z0}^2$. Equilibrium orbits are also characterized by another useful quantity that determines the variation of the axial velocity with the electron energy as [15]

$$d\beta_z / d\gamma = c\Phi / \gamma\gamma_z^2\beta_z\,, \quad (26)$$

$$\Phi = 1 - \frac{(1+\gamma_z^2)\bar{\Omega}_w^2\bar{\omega}_i^2\beta_z^2}{2(\bar{\omega}_i^2 - \gamma\beta_z^2)^3 + 2\bar{\Omega}_w^2\bar{\omega}_i^2\beta_z^2}\,. \quad (27)$$

Φ is positive for the entire range of the group I orbits and the group II orbits with the ion-channel frequency larger than a critical frequency that depends on parameters. For lower ion-channel frequencies, however, Φ is negative, which implies the existence of a negative mass regime in which the axial velocity will increase with decreasing energy. For the chosen parameters, transition from negative Φ (negative mass regime) to the positive Φ takes place at $\bar{\omega}_i/\sqrt{\gamma} = 1.1415$. Since the steady-state amplifier model is considered, the initial amplitude of the vector potential for an un-bunched beam can be selected arbitrarily to represent the amplitude of the injected signal. However, the scalar potential must be chosen from Eq. (22).

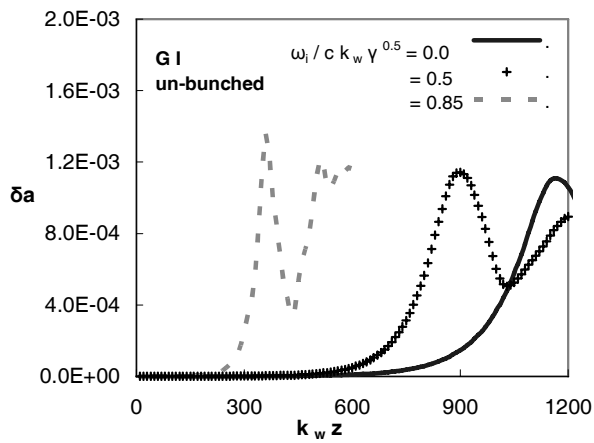

Figure 1: Evolution of radiation amplitude for group I.

The evolution of radiation amplitude with $k_w z$, for a uniform beam is shown in Fig. 1, for the group I orbits, and for $\bar{\omega}_i/\sqrt{\gamma} = 0$ and $\bar{k}_+ = 91.36$ (solid line), $\bar{\omega}_i/\sqrt{\gamma} = 0.5$ and $\bar{k}_+ = 88.82$ (+ mark), and $\bar{\omega}_i/\sqrt{\gamma} = 0.85$ and $\bar{k}_+ = 58.35$ (dashed line).

In this figure two cases of group I orbits are compared with the one without ion-channel. It is seen that after an initial transient phase an extended regime of exponential

growth rate takes place. Afterwards, the radiation field reaches its maximum value when the electrons are trapped at the bottom of the longitudinal potential well. Just before the radiation field saturates, electrons are somewhat spatially bunched, slowed down, and are trapped near the bottom of the wave potential. For the group I orbits, increasing the density of the ion channel, increases the growth rate, decreases the saturation length, and increases the saturated amplitude of the radiation. The reduction of the wave number of the radiation by increasing the ion channel density, but still corresponding to group I orbits, is due to the reduction of the axial velocity.

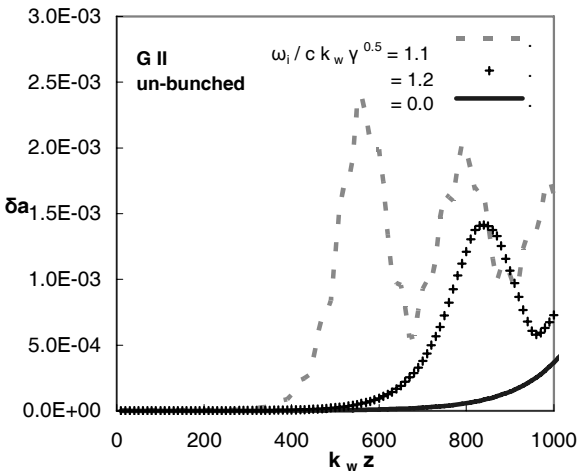

Figure 2: Evolution of radiation amplitude for group II.

The evolution of radiation amplitude with $k_w z$, for a uniform beam for the group II orbits is shown in Fig. 2 for $\bar{\omega}_i/\sqrt{\gamma} = 1.1$ and $\bar{k}_+ = 58.01$ (solid line), $\bar{\omega}_i/\sqrt{\gamma} = 1.2$ and $\bar{k}_+ = 81.30$ (+ mark), and $\bar{\omega}_i/\sqrt{\gamma} = 0$ and $\bar{k}_+ = 91.36$ (dashed line).

In this figure two cases of the group II orbits are compared with the one without ion channel. For the group II orbits, at large ion-channel densities, decreasing the ion-channel density, increases the growth rate, decreases the saturation length, and increases the saturated amplitude of the radiation. It should be noted, that decreasing the ion-channel density, in the group II orbits, is somehow equivalent to increasing the ion-channel density, in the group I orbits, because they both move the electron beam closer to the resonance region [14]. In the negative mass regime of group II orbits, the effect of ion channel is stronger than in both group I orbits and the group II orbits with positive Φ. Increasing the ion-channel density but still corresponding to the group II orbits with $\Phi < 0$, decreases the growth rate and increases the saturation length. For $\bar{\omega}_i/\sqrt{\gamma} = 1.1415$ where $|\Phi| << 1$ the ponderomotive potential vanishes therefore saturation length goes to infinity. This is the transition point between the positive and negative Φ. By increasing the ion-channel density in group II orbits, the radiation wave number increases due to the reduction of the transverse velocity.

CONCLUSION

A local and nonlinear simulation of Raman FEL with planar wiggler and ion channel guiding is presented. The effect of ion channel on saturation length and saturated radiation amplitude is studied. It is shown that ion-channel significantly reduces the saturation length and increases the saturated radiation amplitude. It is worth to state that ion channel is a less expensive alternative to conventional focusing magnets because of lower capital and running cost [2]. Moreover, it allows beam currents higher than the vacuum limit.

ACKNOWLEDGMENT

B. M. would like to thank the Center of Excellence in Computational Aerospace Engineering for financial support.

REFERENCES

[1] Y. P. Bliokh, G. S. Nusinovich, J. Felsteiner, and V. L. Granatstein, Phys. Rev. E 66 (2002) 056503.
[2] K. Takayama and S. Hiramatsu, Phys. Rev. A 37 (1988) 173.
[3] T. Ozaki, K. Ebihara, S. Hiramatsu, Y. Kimura, J. Kishiro, T. Monaka, K. Takayama, and D. H. Whittum, Nucl. Instrum. Methods Phys. Res. A 318 (1992) 101.
[4] L. H. Yu, A. M. Sessler, and D. H. Whittum, Nucl. Instrum. Methods Phys. Res. A 318 (1992) 721.
[5] P. Jha and J. S. Wurtele, Nucl. Instrum. Methods Phys. Res. A 331 (1993) 477.
[6] A. Raghavi, D. N. Giovanni, and H. Mehdian, Nucl. Instrum. Methods Phys. Res. A 591 (2008) 338.
[7] H. P. Freund, Phys. Rev. A 27 (1983) 1977.
[8] N. M. Kroll, P. L. Morton, and M. N. Rosenbluth, IEEE J. Quantum Electron. 17 (1981) 1436.
[9] S. Reiche, Nucl. Instrum. Methods Phys. Res. A 429 (1999) 243.
[10] T. M. Tran and J. S. Wurtele, Phys. Rep. 195 (1990) 1.
[11] D. H. Whittum, A. M. Sessler, and J. M. Dawson, Phys. Rev. Lett. 64 (1990) 2511.
[12] H. P. Freund and J. M. Antonsen, Principle of Free Electron Laser (London, Chapman and Hall, 1996), chapter 5
[13] P. Sprangle, C. M. Tang, and W. M. Manheimer, Phys. Rev. A 21 (1980) 302.
[14] U. H. Hwang, H. Mehdian, J. E. Willett, and Y. M. Aktas Phys. Plasmas 9 (2002) 1010.
[15] H. Mehdian, M. Esmelzadeh, and J. E. Willett, Phys. Plasmas 8 (2001) 3776.